nature ecology & evolution

Brief Communication

https://doi.org/10.1038/s41559-022-01946-1

Acclimation of phenology relieves leaf longevity constraints in deciduous forests

Received: 10 January 2022

Accepted: 2 November 2022

Published online: 12 January 2023

Check for updates

Laura Marqués[1,2,3,4] ✉, Koen Hufkens[1,2,3,4], Christof Bigler[5], Thomas W. Crowther[6], Constantin M. Zohner[6] & Benjamin D. Stocker[1,2,3,4]

Leaf phenology is key for regulating total growing-season mass and energy fluxes. Long-term temporal trends towards earlier leaf unfolding are observed across Northern Hemisphere forests. Phenological dates also vary between years, whereby end-of-season (EOS) dates correlate positively with start-of-season (SOS) dates and negatively with growing-season total net CO_2 assimilation (A_{net}). These associations have been interpreted as the effect of a constrained leaf longevity or of premature carbon (C) sink saturation—with far-reaching consequences for long-term phenology projections under climate change and rising CO_2. Here, we use multidecadal ground and remote-sensing observations to show that the relationships between A_{net} and EOS are opposite at the interannual and the decadal time scales. A decadal trend towards later EOS persists in parallel with a trend towards increasing A_{net}—in spite of the negative A_{net}–EOS relationship at the interannual scale. This finding is robust against the use of diverse observations and models. Results indicate that acclimation of phenology has enabled plants to transcend a constrained leaf longevity or premature C sink saturation over the course of several decades, leading to a more effective use of available light and a sustained extension of the vegetation CO_2 uptake season over time.

For deciduous tree species in temperate and boreal forests, the timing of leaf unfolding in spring and leaf senescence in autumn determines the length of the season during which sunlight is intercepted by leaves, CO_2 is taken up and water is transpired. Start-of-season (SOS) and end-of-season (EOS) dates fluctuate at multiple scales, driven by numerous interacting mechanisms that collectively determine the long-term response to climate change. Dates of leaf phenology vary across climatic[1] and elevational gradients[2]. Long-term temporal trends towards earlier leaf unfolding have been observed across the Northern Hemisphere in remote-sensing data and documented in long-term tree-level observations[3–5]. Such phenological shifts in response to global climate change are altering carbon, water and nutrient cycling and induce feedbacks within the Earth system[6,7].

Relatively reliable models exist to predict SOS on the basis of accumulated temperature and photoperiod[8–11]. In contrast, long-term trends in autumn senescence are less clear[3,12–14], depend on EOS definitions based on senescence start, leaf discolouration stages or dormancy[15,16] and drivers are not well understood[6]. Although experimental evidence exists demonstrating that warm autumn temperatures delay leaf senescence[17], evidence from long-term observations often shows mixed phenology trends[18–20]. This has compromised the development of accurate predictive models and undermines phenology projections under future climate conditions[21–23]. However, a positive correlation between annual SOS and EOS dates has been found in observational[24,25] and experimental studies[17,26], potentially providing useful information for improving EOS predictions. A recent study[27] found an even

[1]Department of Environmental Systems Science, Institute of Agricultural Sciences, ETH Zurich, Zurich, Switzerland. [2]Swiss Federal Institute for Forest, Snow and Landscape Research WSL, Birmensdorf, Switzerland. [3]Institute of Geography, University of Bern, Bern, Switzerland. [4]Oeschger Centre for Climate Change Research, University of Bern, Bern, Switzerland. [5]Department of Environmental Systems Science, Institute of Terrestrial Ecosystems, ETH Zurich, Zurich, Switzerland. [6]Department of Environmental Systems Science, Institute of Integrative Biology, ETH Zurich, Zurich, Switzerland. ✉e-mail: laura.marques@usys.ethz.ch

stronger relationship between observed EOS and simulated A_{net}, such that greater productivity was associated with earlier leaf senescence. This negative relationship between growing-season total net CO_2 assimilation (A_{net}) and EOS was interpreted as an expression of plant C sink saturation[26,28,29], whereby an early replenishment of non-structural carbon reserves induces an early cessation of the photosynthetically active season. An EOS advancement over the second half of the twenty-first century was thus predicted as a consequence of accelerated C sink saturation due to continued SOS advances and enhanced photosynthesis under rising CO_2 levels[27]. However, in the past, a sustained SOS advance[3] and a widely observed CO_2-driven increase in photosynthesis[30–33] did not lead to a corresponding advance in EOS[3]. With these interacting mechanisms operating over different spatiotemporal scales[34] and the influence of their associated environmental controls, it has been challenging to disentangle drivers and identify general trends in the changes in autumn leaf senescence.

Here, we investigated this apparent conflict by decomposing long-term trends, interannual and spatial variations using linear mixed-effects models (LMMs). We hypothesized that the relationships between A_{net} and EOS are driven by multiple processes and are non-stationary over decadal time scales. We complemented the analysis of multiyear ground observations (1948–2015) from the PEP725 dataset[5] of 434,226 European tree-level phenology observations with an analysis of remotely sensed phenological dates to expand the extent of data coverage in spatial and climatic space. Remotely sensed estimates of phenology (2001–2018) were obtained from MODIS MCD12Q2 Collection 6 (refs. [35,36]) for 4,879 randomly sampled points of deciduous tree species in temperate and boreal forests in the Northern Hemisphere. We performed all analyses with A_{net} estimates generated using a comprehensively evaluated photosynthesis model[37] and explored the robustness of the estimates and respective statistical models by using A_{net} estimates as previously used by ref. [27]. We used model-based A_{net} estimates because no data are available for the locations providing the PEP725 and MODIS phenology observations. Additionally, we used observation-based ecosystem-level CO_2 assimilation to evaluate the robustness of the identified photosynthesis–EOS relationships. Observations were based on daily gross primary production (GPP) estimates from eddy covariance measurements (FLUXNET 2015 Tier 1; ref. [38]) for 32 sites, paired with MODIS phenology data, extracted for the respective sites. See Methods for a detailed account of the analysis, data and modelling.

We found opposing A_{net}–EOS relationships at different temporal scales. When controlling for the effect of A_{net}, we found a clear decadal-scale trend component towards later EOS (0.117 ± 0.002 d yr^{-1}, representing the mean ± the standard error; Fig. 1a). After separating the long-term trend, the remaining A_{net}–EOS relationship reflects interannual variations. At this scale, A_{net} is negatively correlated with EOS (−0.011 ± 0.000 d (gC m^{-2} yr^{-1})$^{-1}$; Fig. 1b)—with stronger effects than those based on a univariate model (−0.003 ± 0.000 d (gC m^{-2} yr^{-1})$^{-1}$; Fig. 1c). The net effect of these opposing relationships is a relatively small, yet significant, delay in EOS over time of 0.046 ± 0.001 d yr^{-1} (Extended Data Fig. 1a)—in spite of the steadily increasing A_{net} since the mid-twentieth century (6.456 ± 0.011 gC m^{-2} yr^{-2}; Extended Data Fig. 1b). These results are qualitatively robust against the use of alternative A_{net} estimates[39], both in terms of the long-term trend towards later autumn senescence (0.252 ± 0.001 d yr^{-1}; Extended Data Fig. 2a) and in terms of the negative effect of interannual A_{net} variations (−0.076 ± 0.000 d (gC m^{-2} yr^{-1})$^{-1}$; Extended Data Fig. 2b)—in agreement with results based on the univariate model (−0.064 ± 0.000 d (gC m^{-2} yr^{-1})$^{-1}$; Extended Data Fig. 2c)[27]. The parallel gradual A_{net} increase and long-term trend towards delayed autumn senescence are suggestive of a positive long-term A_{net}–EOS relationship—opposite to the negative relationship at the interannual time scale. A sensitivity analysis confirmed the robustness of these results also when considering different end dates to define the cumulative growing-season A_{net} (Extended Data Fig. 3).

Scale-dependent relationship reversals were also found when decomposing interannual variations from spatial variations; that is, when separating annual anomalies from multiyear means by site in LMMs. Due to relatively limited temporal coverage of the remote-sensing data (2001–2018), we did not separate a long-term trend. Across space, higher mean A_{net} is associated with later mean EOS (0.033 ± 0.000 d (gC m^{-2} yr^{-1})$^{-1}$; Fig. 2a,c,d), while the opposite relationship prevails in response to interannual A_{net} variations at a given location (−0.010 ± 0.000 d (gC m^{-2} yr^{-1})$^{-1}$; Fig. 2b). Results remained robust under multiple thresholds to define the growing season and estimate A_{net} (sensitivity analysis in Extended Data Fig. 4). The same patterns were identified also when conducting a corresponding analysis using observational data for a subset of sites for which estimates of ecosystem-level CO_2 assimilation are provided by eddy covariance flux measurements. We found a positive relationship between observed mean growing-season GPP and EOS (0.028 ± 0.016 d (gC m^{-2} yr^{-1})$^{-1}$; Extended Data Fig. 5a), supporting the robustness of the patterns found on the basis of modelled ecosystem-level GPP (0.044 ± 0.027 d (gC m^{-2} yr^{-1})$^{-1}$; Extended Data Fig. 5c) and modelled ecosystem-level GPP minus dark respiration (0.049 ± 0.028 d (gC m^{-2} yr^{-1})$^{-1}$; Extended Data Fig. 6a) from simulations performed for the sites of eddy covariance measurements. When considering interannual GPP variations at a given site, observations did not show a negative effect (Extended Data Fig. 5b), in contrast to simulations (Extended Data Figs. 5d and 6b), although relationships were non-significant in all cases.

These relationships yield several insights into potential processes underlying phenology shifts under global environmental change. A link between interannual variations of A_{net} and EOS emerges from both the ground-based and remote-sensing-based analyses. Since A_{net} represents the cumulative net CO_2 assimilation since SOS, the A_{net}–EOS relationship is closely related to the previously reported relationship between SOS and EOS[17,24–26]. Early leaf unfolding leading to early senescence has been hypothesized to be the result of a relatively constant length of leaf phenological stages[40] or of a leaf aging effect[41–43], whereby a tightly constrained leaf longevity implies direct control of SOS on EOS[24]. Given the well-documented gradual SOS advancement[44–48] (−0.198 ± 0.001 d yr^{-1}; Extended Data Fig. 1d), this process should induce an advancement also of EOS. However, our analysis reveals that this has not been the case (0.071 ± 0.001 d yr^{-1}; Extended Data Fig. 7a), as earlier mean SOS was associated with later EOS across space (Extended Data Fig. 8a). Similarly, the strong relationship between A_{net}–EOS, apparent at the interannual scale, has not been stationary over several decades. This indicates that the interplay between multiple drivers and processes has resulted in a gradual relief of tight constraints relevant at the interannual time scale, which potentially arise from premature leaf aging or C sink saturation. We interpret this non-stationarity of the A_{net}–EOS and the SOS–EOS relationships as being reflective of acclimation—an adjustment of an individual to an environmental change that is manifested as alterations in the short-term response function of physiological processes[49].

What are the drivers of observed phenological relationships and their acclimation? If the negative interannual A_{net}–EOS relationship was due to C sink saturation, it should prevail also in the long-term, as photosynthetic CO_2 assimilation is enhanced under rising atmospheric CO_2 (refs. [30–33]). However, it appears that the tight constraints, apparent at the interannual scale, are relieved over several decades. The opposing relationships at different scales found here question the prediction that gradual increases in photosynthesis cause a progressive advancement of EOS by earlier C sink saturation. Previous studies have generally demonstrated a thermal control delaying EOS across spatial gradients and years[50]. Rising autumn temperatures, causing a slow-down of chlorophyll degradation and leaf discoloration[15], have been suggested to underlie trends and are considered in autumn senescence models[51]. Most warming experiments have also shown later EOS for various deciduous tree species[52]. Further insights

https://doi.org/10.1038/s41559-022-01946-1

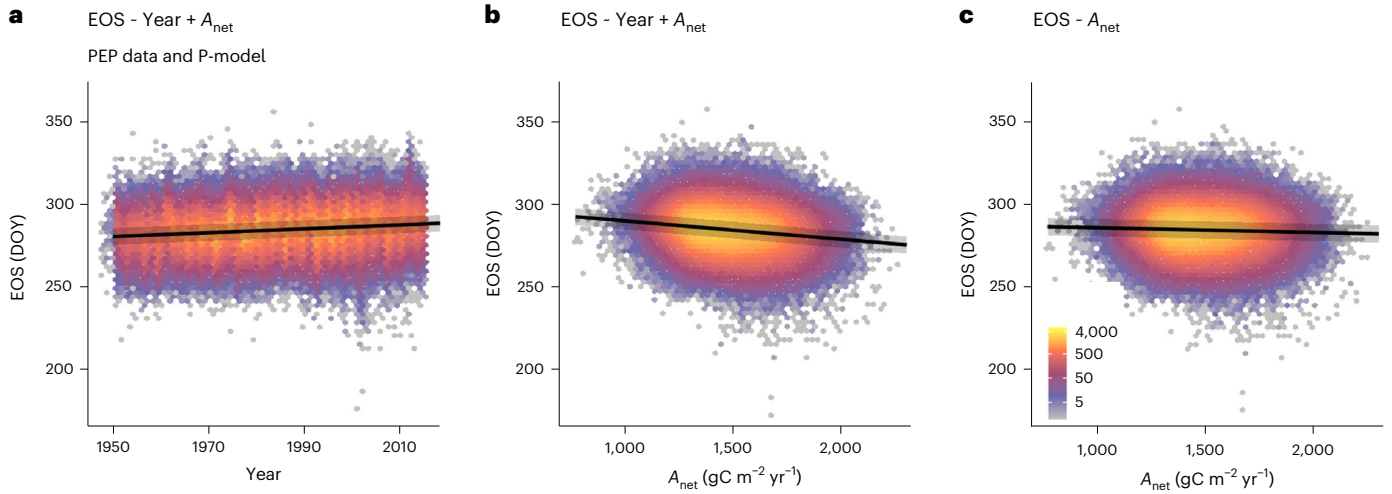

Fig. 1 | Relationship of CO_2 assimilation and autumn phenology from ground observations. a,**b**, Partial relationships of a multiple LMM, where EOS is the response variable and the long-term trend (year) (**a**) and A_{net} (**b**) are treated as fixed effects. **c**, EOS versus A_{net} based on an LMM with A_{net} as a single fixed effect. A_{net} estimates are simulated by the P-model. In both bivariate and univariate models, site and species are treated as grouping variables of random intercepts. Black lines represent the expected mean values from LMMs and grey ranges their 95% confidence intervals. Colour hexagonal heatmap represents the observed data adjusted for the effects of the covariates.

into the importance of a potential C sink saturation mechanism causing a reversal of effects by warming autumn temperatures will be gained by linking observations of non-structural C dynamics with autumn phenology. Our results indicate that different mechanisms and environmental controls are at play at different temporal scales, potentially undermining long-term projections that are informed by short-term variations of autumn phenology.

Why does a negative relationship between A_{net} and EOS emerge when the long-term trend and the spatial variation are not separated in LMMs? A possible explanation is that relatively large interannual phenology variations dominate over the smaller long-term temporal pattern in the data we analysed and mask their effect in univariate models. Indeed, separating the opposing long-term and spatial trends from the remaining component of interannual variations improves model performance significantly (based on $P < 0.001$ in analysis of variance and lower Akaike information criterion) and increases the strength of their interannual links in all models (see estimates for bivariate and univariate models in Supplementary Table 1). This provides further support for an important mechanism underlying interannual autumn phenology variations. However, it also indicates that this does not preclude the existence of other interacting mechanisms that enable an acclimating response which is revealed here to have been occurring over the past decades. The net effect of opposing mechanisms, apparent in the univariate models, is subject to the data and their relative magnitudes of variations across multiple scales.

The long-term and spatial relationships between A_{net} and EOS (and between SOS and EOS) are qualitatively consistent and the patterns of simulated mean GPP agree with those extracted from observations. This indicates that the phenology of individual trees has acclimated over the course of decades in the same direction as evident from the spatial analysis (high A_{net} occurs in places with late EOS; Fig. 2c,d). Note that the long-term temporal trends derived from tree-level observations in the PEP725 data emerge within individual species observed at different locations, while spatial variations may arise also as a result of varying species composition across space and of adaptation within populations of a given species. Our results, therefore, suggest a clear plasticity of autumn phenology over time, mirroring effects by species distribution and long-term adaptation of individuals and plant communities growing along a large climatic gradient. This indicates a trend towards climate-adapted and potentially optimal functioning.

Opposing relationships at different time scales and across the Northern Hemisphere reconcile apparent conflicts by the reported negative A_{net}–EOS relationship but absent shifts towards earlier EOS as A_{net} has increased over past decades. Our analyses indicate that a gradual acclimation of plant physiology and phenology has enabled plants to transcend a constrained leaf longevity or a stationary C sink saturation effect, evident from the clear short-term SOS–EOS and A_{net}–EOS relationships. Thus, in the long run, plants may assimilate more CO_2 without a direct and inescapable penalty by earlier leaf senescence and without thus foregoing late-season carbon assimilation. This apparent plasticity in phenology appears to have driven plants towards optimal functioning in a changing climate.

Methods

Pan European observational data (PEP725)

Spring and autumn phenology dates were collected from the Pan European Phenology Project[5], which provides in situ observations for Europe. Phenology dates were defined following the BBCH (Biologische Bundesanstalt, Bundessortenamt und Chemische Industrie) codes (phenophases). Different phenophases were considered to define both SOS and EOS to increase the number of sites in the study. Leaf-out was defined as the date when the first (BBCH11) or 50% of leaf stalks are visible (BBCH13) for the deciduous angiosperms and as the date when the first leaves separated (BBCH10) for the deciduous conifers. Leaf senescence was defined as the date when 50% of leaves had lost their green colour (BBCH94) or had fallen (BCCH95). Data cleaning consisted of removing time series with <15 years of observations, dates deviating more than three times the median absolute deviation from the median and time series for which the standard deviation of phenological observations across years was >15 for SOS and 20 for EOS[27]. The dataset resulted in 3,855 sites across Central Europe (Extended Data Fig. 9a) with 14,626 individual time series and 434,226 phenological observations between 1948 and 2015.

MODIS phenology data

We used the MODIS C6 MCD12Q2 land surface dynamics product[35] which provides land surface phenological data at 500 m spatial resolution from 2001 to 2018, derived from time series of the two-band enhanced vegetation index (EVI2) and calculated from MODIS nadir bidirectional reflectance distribution function adjusted surface

https://doi.org/10.1038/s41559-022-01946-1

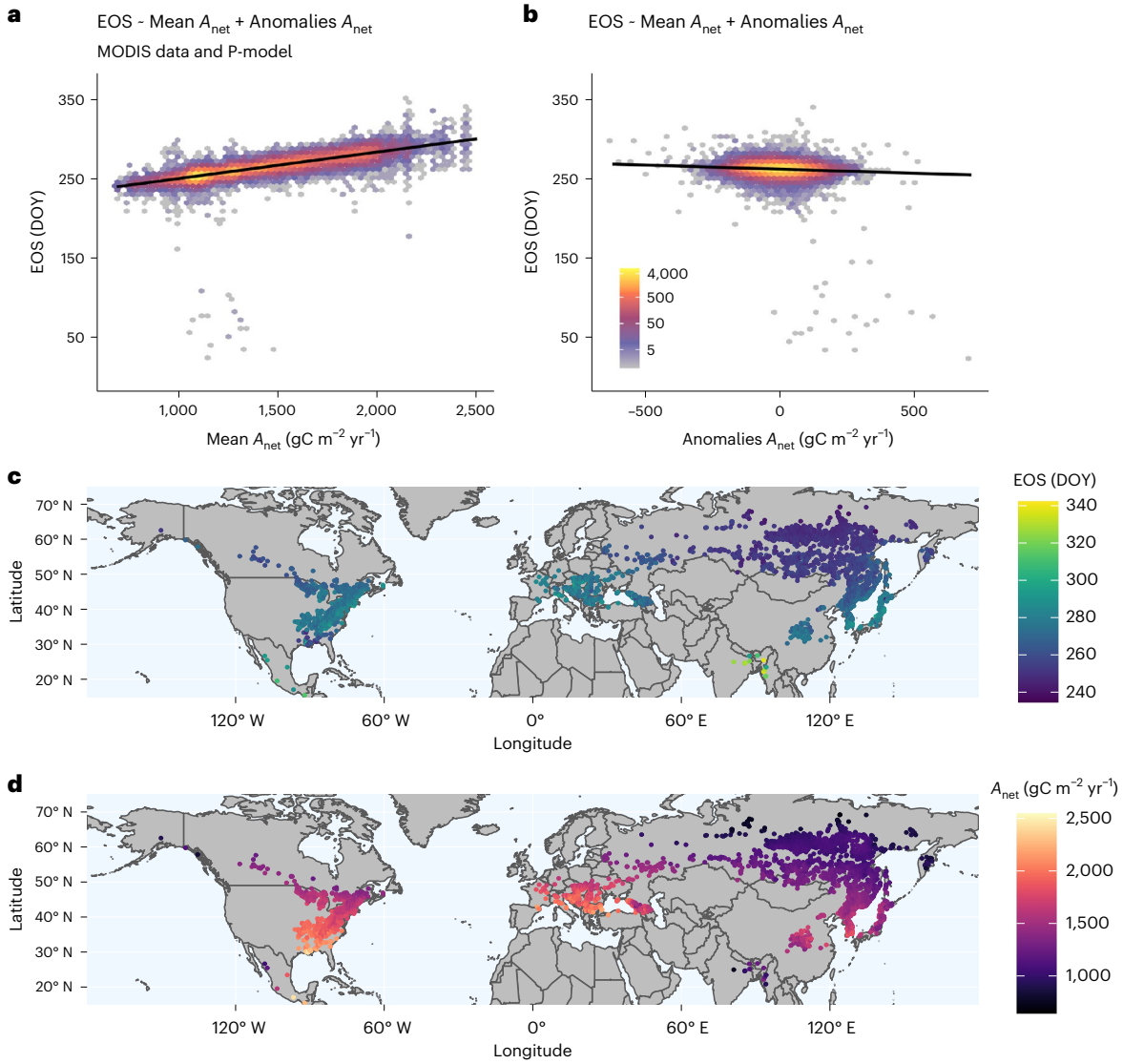

Fig. 2 | Relationships of CO_2 assimilation and autumn phenology from remote-sensing observations. a,**b**, Partial relationships of a multiple LMM, where EOS is the response variable and mean A_{net} (**a**) and anomalies A_{net} (**b**) relative to the mean value are treated as fixed effects, while site and year are treated as grouping variables of random intercepts. A_{net} estimates are simulated by the P-model. Black lines represent the expected mean values from LMMs and grey ranges their 95% confidence intervals. Colour hexagonal heatmap represents the observed data adjusted for the effects of the covariates. **c**,**d**, Mean values of EOS (**c**) and A_{net} (**d**) for grid cells distributed along the Northern Hemisphere. Colour points represent the EOS observations and A_{net} simulations.

reflectance (NBAR-EVI2)[36,53]. From this product, leaf-out was taken as the midgreenup point, that is, the date when EVI2 first crossed 50% of the segment EVI2 amplitude. Leaf senescence was taken as the midgreendown point, that is, the date when EVI2 last crossed 50% of the segment EVI2 amplitude. We selected the midgreenup and midgreendown to define SOS and EOS instead of the greenup and dormancy following the recommendations from the MCD12Q2 product user guide to capture the season start and end in high-latitude regions. Data were downloaded using the MODISTools R package[54]. We randomly sampled 5,000 pixels spread evenly between temperate broadleaf and needleleaf deciduous forests following the International Geosphere–Biosphere Programme (IGBP) classes and selected the points corresponding to the Northern Hemisphere (4,879; Extended Data Fig. 9b).

Photosynthesis estimation

For locations where tree-level phenology observations were available from the PEP725 data, we used two alternative estimates of A_{net}. Results shown in Fig. 1 are based on simulated A_{net} using the P-model[37]. Results shown in Extended Data Fig. 2 are based on A_{net} as estimated by ref. [27] using their implementation of the LPJ model[39]. In both cases, A_{net} estimates represent gross assimilation minus dark respiration. The P-model is a big-leaf model for simulating CO_2 assimilation based on Farquhar–von Caemmerer–Berry photosynthesis kinetics[55] and an eco-evolutionary optimality principle for the acclimation of photosynthetic capacities[56] and is implemented by the rsofun R package[57]. The same P-model-based approach was applied for estimating cumulative A_{net} at locations where phenology data were extracted from the MODIS remote-sensing product and results are shown in Fig. 2. The cumulative growing-season net photosynthesis was obtained by summing the daily A_{net} for all days of the growing season, starting at the date of observed SOS and ending on the date when daylength falls below 11.2 h. Thus, cumulative A_{net} is independent of EOS. We additionally conducted a sensitivity analysis to test the importance of the length of the growing season, considering a daylength threshold of 10.0 h and two different fixed days-of-year on 23 September and on 21 June. In the P-model, the photosynthetically active radiation (PAR) is based

on shortwave radiation from WATCH-WFDEI[58], using a constant of 2.04 (μmol J^{-1}; ref. [59]) and spatially downscaled using the WorldClim2 (ref. [60]) monthly climatology. We assumed a fraction of absorbed PAR (fAPAR) of 1.0 for all sites and dates between their respectively observed SOS and EOS dates. Hence, A_{net} represents the leaf-level net CO_2 assimilation and is representative of conditions in full light. A seasonal course of photosynthetic capacities and leaf-level radiation use efficiency is simulated by the P-model. Also, other meteorological forcing data for P-model simulations were taken from WATCH-WFDEI[58], downscaled using WorldClim2 (ref. [60]) as implemented by the ingestr R package[61]. Details of the theory underlying the P-model are described in refs. [37,62].

Data analysis

We fitted LMMs to investigate the relationships between autumn phenology, net photosynthesis and spring leaf-out. We specified models to separate the interannual, long-term and spatial components of variation. The general structure of the models can be summarized as:

$$Y = X\boldsymbol{a} + Z\boldsymbol{b} + \varepsilon$$

where Y represents the response variable (for example, EOS, expressed as day-of-year), a is the vector of fixed effects, b is the vector of random intercepts, X and Z are regression matrices of fixed and random effects, respectively, and ε is the within-group error term. For performing the temporal analyses, the predictor variables (for example, A_{net}, SOS and year) were standardized and site and species were treated as grouping variables of random intercepts. Since consistent phenophases were used within sites but phenophases used may vary between sites, the treatment of site ID as a grouping variable for random intercepts implicitly accounts for systematic offsets between different phenophases. For performing the spatial analysis, we calculated the mean and standard deviation values of the predictors (for example, A_{net} and SOS) and evaluated their effects on EOS. Site and year were treated as grouping variables of random intercepts for spatial analyses with MODIS data. Residuals of the models were checked for normality and homoscedasticity. Figures 1 and 2 and Extended Data Figs. 1–4, 7 and 8 represent the partial residual plots, that is, the observed data adjusted for the effects of the covariates alongside the model fit. The main statistics of the LMMs and the sensitivity analysis are displayed in Supplementary Tables 1 and 2, respectively. LMMs were fitted using the lme4 R package[63]. The analyses were performed using the *R* statistical software v.4.0.5 (ref. [64]).

Support from photosynthesis observations

We obtained ecosystem-level CO_2 assimilation data from global eddy covariance towers (FLUXNET 2015 Tier 1)[38]. We used daily GPP data (named GPP_NT_VUT_REF in the database) and thus calculated gross ecosystem-level CO_2 assimilation, that is, GPP not discounted for any respiration. We focused on ecosystems classified as broadleaf deciduous, needleleaf deciduous and mixed forests on the basis of the IGBP definition. This selection resulted in 32 sites with 50% of the data covering at least 10 yr (Supplementary Table 3). To assess the robustness of phenology–photosynthesis relationships found with model-based analyses, we ran the P-model[37] for the selected flux sites using locally measured meteorological conditions as model forcing and fAPAR data gathered from remote-sensing products (MODIS MCD15A3H)[65]. Since the observational data provide information on gross ecosystem-level CO_2 assimilation, we considered the modelled GPP without discounting for dark respiration. To assess the effects of this discounting, we also used modelled GPP minus ecosystem-level dark respiration. Site-level GPP data were paired with remotely sensed phenology observations from the MODIS C6 MCD12Q2 product (available for the period 2001–2018) using the same autumn phenology definitions as described above. The observed and simulated cumulative GPP and GPP minus ecosystem-level dark respiration were calculated from days starting at the observed SOS and ending on the date when daylength falls below 11.2 h. We then separated multiyear means by site from interannual variations to investigate the relationships between autumn phenology and both the observed and simulated photosynthesis. Extended Data Figures 5 and 6 represent the partial relationships of multiple LMMs when considering either GPP or GPP minus ecosystem-level dark respiration.

Reporting summary

Further information on research design is available in the Nature Portfolio Reporting Summary linked to this article.

Data availability

Ground phenology data provided by the members of the PEP725 project are freely available at http://www.pep725.eu. Remote-sensing phenology data from the MODIS C6 MCD12Q2 land surface dynamics product are freely accessible at https://lpdaac.usgs.gov/products/mcd12q2v006/. Eddy covariance data are freely available by the FLUXNET community at https://fluxnet.org.

Code availability

Code for the data analysis of this study is available at the Github repository https://zenodo.org/record/7245870.

References

1. Peaucelle, M. et al. Spatial variance of spring phenology in temperate deciduous forests is constrained by background climatic conditions. *Nat. Commun.* **10**, 5388 (2019).
2. Hopkins, A. D. The bioclimatic law. *Mon. Weather Rev.* **48**, 355–355 (1920).
3. Piao, S. et al. Plant phenology and global climate change: current progresses and challenges. *Glob. Change Biol.* **25**, 1922–1940 (2019).
4. Ge, Q., Wang, H., Rutishauser, T. & Dai, J. Phenological response to climate change in China: a meta-analysis. *Glob. Change Biol.* **21**, 265–274 (2015).
5. Templ, B. et al. Pan European Phenological database (PEP725): a single point of access for European data. *Int. J. Biometeorol.* **62**, 1109–1113 (2018).
6. Richardson, A. D. et al. Climate change, phenology, and phenological control of vegetation feedbacks to the climate system. *Agric. For. Meteorol.* **169**, 156–173 (2013).
7. Morisette, J. T. et al. Tracking the rhythm of the seasons in the face of global change: phenological research in the 21st century. *Front. Ecol. Environ.* **7**, 253–260 (2009).
8. Flynn, D. F. B. & Wolkovich, E. M. Temperature and photoperiod drive spring phenology across all species in a temperate forest community. *New Phytol.* **219**, 1353–1362 (2018).
9. Peñuelas, J., Rutishauser, T. & Filella, I. Phenology feedbacks on climate change. *Science* **324**, 887–888 (2009).
10. Körner, C. & Basler, D. Plant science. *Phenol. Glob. Warm. Sci.* **327**, 1461–1462 (2010).
11. Delpierre, N. et al. Temperate and boreal forest tree phenology: from organ-scale processes to terrestrial ecosystem models. *Ann. For. Sci.* **73**, 5–25 (2016).
12. Klosterman, S. T. et al. Evaluating remote sensing of deciduous forest phenology at multiple spatial scales using PhenoCam imagery. *Biogeosciences* **11**, 4305–4320 (2014).
13. Hufkens, K. et al. Linking near-surface and satellite remote sensing measurements of deciduous broadleaf forest phenology. *Remote Sens. Environ.* **117**, 307–321 (2012).
14. Garrity, S. R. et al. A comparison of multiple phenology data sources for estimating seasonal transitions in deciduous forest carbon exchange. *Agric. For. Meteorol.* **151**, 1741–1752 (2011).
15. Fracheboud, Y. et al. The control of autumn senescence in European aspen. *Plant Physiol.* **149**, 1982–1991 (2009).

16. Mariën, B. et al. Does drought advance the onset of autumn leaf senescence in temperate deciduous forest trees? *Biogeosciences* **18**, 3309–3330 (2021).
17. Fu, Y. H. et al. Larger temperature response of autumn leaf senescence than spring leaf-out phenology. *Glob. Change Biol.* **24**, 2159–2168 (2018).
18. Menzel, A., Sparks, T. H., Estrella, N. & Roy, D. B. Altered geographic and temporal variability in phenology in response to climate change. *Glob. Ecol. Biogeogr.* **15**, 498–504 (2006).
19. Gordo, O. & Sanz, J. J. Long-term temporal changes of plant phenology in the Western Mediterranean. *Glob. Change Biol.* **15**, 1930–1948 (2009).
20. Meier, M., Vitasse, Y., Bugmann, H. & Bigler, C. Phenological shifts induced by climate change amplify drought for broad-leaved trees at low elevations in Switzerland. *Agric. For. Meteorol.* **307**, 108485 (2021).
21. Basler, D. Evaluating phenological models for the prediction of leaf-out dates in six temperate tree species across central Europe. *Agric. For. Meteorol.* **217**, 10–21 (2016).
22. Keenan, T. F. et al. Terrestrial biosphere model performance for inter-annual variability of land–atmosphere CO_2 exchange. *Glob. Change Biol.* **18**, 1971–1987 (2012).
23. Liu, G., Chen, X., Fu, Y. & Delpierre, N. Modelling leaf coloration dates over temperate China by considering effects of leafy season climate. *Ecol. Modell.* **394**, 34–43 (2019).
24. Keenan, T. F. & Richardson, A. D. The timing of autumn senescence is affected by the timing of spring phenology: implications for predictive models. *Glob. Change Biol.* **21**, 2634–2641 (2015).
25. Wu, C., Hou, X., Peng, D., Gonsamo, A. & Xu, S. Land surface phenology of China's temperate ecosystems over 1999–2013: spatial–temporal patterns, interaction effects, covariation with climate and implications for productivity. *Agric. For. Meteorol.* **216**, 177–187 (2016).
26. Fu, Y. S. H. et al. Variation in leaf flushing date influences autumnal senescence and next year's flushing date in two temperate tree species. *Proc. Natl Acad. Sci. USA* **111**, 7355–7360 (2014).
27. Zani, D., Crowther, T. W., Mo, L., Renner, S. S. & Zohner, C. M. Increased growing-season productivity drives earlier autumn leaf senescence in temperate trees. *Science* **370**, 1066–1071 (2020).
28. Paul, M. J. & Foyer, C. H. Sink regulation of photosynthesis. *J. Exp. Bot.* **52**, 1383–1400 (2001).
29. Herold, A. Regulation of photosynthesis by sink activity—the missing link. *New Phytol.* **86**, 131–144 (1980).
30. Keenan, T. F. et al. Recent pause in the growth rate of atmospheric CO_2 due to enhanced terrestrial carbon uptake. *Nat. Commun.* **7**, 13428 (2016).
31. Campbell, J. E. et al. Large historical growth in global terrestrial gross primary production. *Nature* **544**, 84–87 (2017).
32. Schimel, D., Stephens, B. B. & Fisher, J. B. Effect of increasing CO_2 on the terrestrial carbon cycle. *Proc. Natl Acad. Sci.USA* **112**, 436–441 (2015).
33. Walker, A. P. et al. Integrating the evidence for a terrestrial carbon sink caused by increasing atmospheric CO. *New Phytol.* **229**, 2413–2445 (2021).
34. Liu, Q. et al. Modeling leaf senescence of deciduous tree species in Europe. *Glob. Change Biol.* **26**, 4104–4118 (2020).
35. Friedl, M., Gray, J. & Sulla-Menashe, D. *MCD12Q2 MODIS/Terra+Aqua Land Cover Dynamics Yearly L3 Global 500m SIN Grid V006* (NASA, 2019).
36. Zhang, X. et al. Monitoring vegetation phenology using MODIS. *Remote Sens. Environ.* **84**, 471–475 (2003).
37. Stocker, B. D. et al. P-model v1.0: an optimality-based light use efficiency model for simulating ecosystem gross primary production. Geosci. *Model Dev.* **13**, 1545–1581 (2020).
38. Pastorello, G. et al. The FLUXNET2015 dataset and the ONEFlux processing pipeline for eddy covariance data. *Sci. Data* **7**, 225 (2020).
39. Sitch, S. et al. Evaluation of ecosystem dynamics, plant geography and terrestrial carbon cycling in the LPJ dynamic global vegetation model. *Glob. Change Biol.* **9**, 161–185 (2003).
40. Hänninen, H. & Tanino, K. Tree seasonality in a warming climate. *Trends Plant Sci.* **16**, 412–416 (2011).
41. Kikuzawa, K. & Lechowicz, M. J. *Ecology of Leaf Longevity* (Springer, 2011).
42. Fu, Y. H. et al. Nutrient availability alters the correlation between spring leaf-out and autumn leaf senescence dates. *Tree Physiol.* **39**, 1277–1284 (2019).
43. Lim, P. O., Kim, H. J. & Nam, H. G. Leaf senescence. *Annu. Rev. Plant Biol.* **58**, 115–136 (2007).
44. Piao, S., Friedlingstein, P., Ciais, P., Viovy, N. & Demarty, J. Growing season extension and its impact on terrestrial carbon cycle in the Northern Hemisphere over the past 2 decades. *Glob. Biogeochem. Cycles* **21**, GB3018 (2007).
45. Jeong, S.-J., Ho, C.-H., Gim, H.-J. & Brown, M. E. Phenology shifts at start vs. end of growing season in temperate vegetation over the Northern Hemisphere for the period 1982–2008. *Glob. Change Biol.* **17**, 2385–2399 (2011).
46. Cong, N. et al. Changes in satellite-derived spring vegetation green-up date and its linkage to climate in China from 1982 to 2010: a multimethod analysis. *Glob. Change Biol.* **19**, 881–891 (2013).
47. Keenan, T. F. et al. Net carbon uptake has increased through warming-induced changes in temperate forest phenology. *Nat. Clim. Change* **4**, 598–604 (2014).
48. Garonna, I., de Jong, R. & Schaepman, M. E. Variability and evolution of global land surface phenology over the past three decades (1982–2012). *Glob. Change Biol.* **22**, 1456–1468 (2016).
49. Smith, N. G. & Dukes, J. S. Plant respiration and photosynthesis in global-scale models: incorporating acclimation to temperature and CO_2. *Glob. Change Biol.* **19**, 45–63 (2013).
50. Estiarte, M. & Peñuelas, J. Alteration of the phenology of leaf senescence and fall in winter deciduous species by climate change: effects on nutrient proficiency. *Glob. Change Biol.* **21**, 1005–1017 (2015).
51. Delpierre, N. et al. Modelling interannual and spatial variability of leaf senescence for three deciduous tree species in France. *Agric. For. Meteorol.* **149**, 938–948 (2009).
52. Chung, H. et al. Experimental warming studies on tree species and forest ecosystems: a literature review. *J. Plant Res.* **126**, 447–460 (2013).
53. Schaaf, C. B. et al. First operational BRDF, albedo nadir reflectance products from MODIS. *Remote Sens. Environ.* **83**, 135–148 (2002).
54. Tuck, S. L. et al. MODISTools—downloading and processing MODIS remotely sensed data in R. *Ecol. Evol.* **4**, 4658–4668 (2014).
55. Farquhar, G. D., von Caemmerer, S. & Berry, J. A. A biochemical model of photosynthetic CO_2 assimilation in leaves of C3 species. *Planta* **149**, 78–90 (1980).
56. Medlyn, B. E. et al. Reconciling the optimal and empirical approaches to modelling stomatal conductance. *Glob. Change Biol.* **17**, 2134–2144 (2011).
57. Stocker, B. rsofun: A modelling framework that implements the P-model for leaf-level acclimation of photosynthesis. R package version 4.3 https://github.com/computationales/rsofun (2020).
58. Weedon, G. P. et al. The WFDEI meteorological forcing data set: WATCH Forcing Data methodology applied to ERA-Interim reanalysis data. *Water Resour. Res.* **50**, 7505–7514 (2014).
59. Meek, D. W., Hatfield, J. L., Howell, T. A., Idso, S. B. & Reginato, R. J. A generalized relationship between photosynthetically active radiation and solar radiation 1. *Agron. J.* **76**, 939–945 (1984).

60. Fick, S. E. & Hijmans, R. J. WorldClim 2: new 1-km spatial resolution climate surfaces for global land areas. *Int. J. Climatol.* **37**, 4302–4315 (2017).
61. Stocker, B. ingestr: A tool to extract environmental point data from large global files or remote data servers. R package version 1.4 https://github.com/computationales/ingestr (2020).
62. Wang, H. et al. Towards a universal model for carbon dioxide uptake by plants. *Nat. Plants* **3**, 734–741 (2017).
63. Bates, D., Mächler, M., Bolker, B. & Walker, S. Fitting linear mixed-effects models using lme4. *J. Stat. Softw.* **67**, 1–48 (2015).
64. R Core Team. *R: A Language and Environment for Statistical Computing* (R Foundation for Statistical Computing, 2021).
65. Myneni, R., Knyazikhin, Y. & Park, T. *MCD15A3H MODIS/Terra+Aqua Leaf Area Index/FPAR 4-day L4 Global 500m SIN Grid V006* (NASA EOSDIS Land Processes DAAC, 2015).

Acknowledgements

We thank T. Keenan, J. Madrigal-González, H. Bugmann, M. Meier and Y. Vitasse for their valuable feedback on the study. L.M. and B.D.S. were funded by the Swiss National Science Foundation grant no. PCEFP2_181115. K.H. was supported by the generosity of E. and W. Schmidt by recommendation of the Schmidt Futures programme. C.M.Z. was funded by the Ambizione grant PZ00P3_193646. Ground phenology data were provided by the members of the PEP725 project. This work used eddy covariance data acquired and shared by the FLUXNET community, including these networks: AmeriFlux, AfriFlux, AsiaFlux, CarboAfrica, CarboEuropeIP, CarboItaly, CarboMont, ChinaFlux, Fluxnet-Canada, GreenGrass, ICOS, KoFlux, LBA, NECC, OzFlux-TERN, TCOS-Siberia and USCCC. The FLUXNET eddy covariance data processing and harmonization was carried out by the ICOS Ecosystem Thematic Center, AmeriFlux Management Project and Fluxdata project of FLUXNET, with the support of CDIAC and the OzFlux, ChinaFlux and AsiaFlux offices.

Author contributions

B.D.S. and L.M. conceived and developed the study. B.D.S., K.H. and L.M. gathered the MODIS data, ran the P-model simulations and conducted the statistical analyses. L.M. and B.D.S. led the writing of the manuscript. C.B. contributed critically to the analyses and the writing. C.M.Z. and T.W.C. gave substantial inputs to the manuscript. All authors gave final approval for publication.

Competing interests

The authors declare no competing interests.

Additional information

Extended data is available for this paper at https://doi.org/10.1038/s41559-022-01946-1.

Supplementary information The online version contains supplementary material available at https://doi.org/10.1038/s41559-022-01946-1.

Correspondence and requests for materials should be addressed to Laura Marqués.

Peer review information *Nature Ecology & Evolution* thanks the anonymous reviewers for their contribution to the peer review of this work. Peer reviewer reports are available.

https://doi.org/10.1038/s41559-022-01946-1

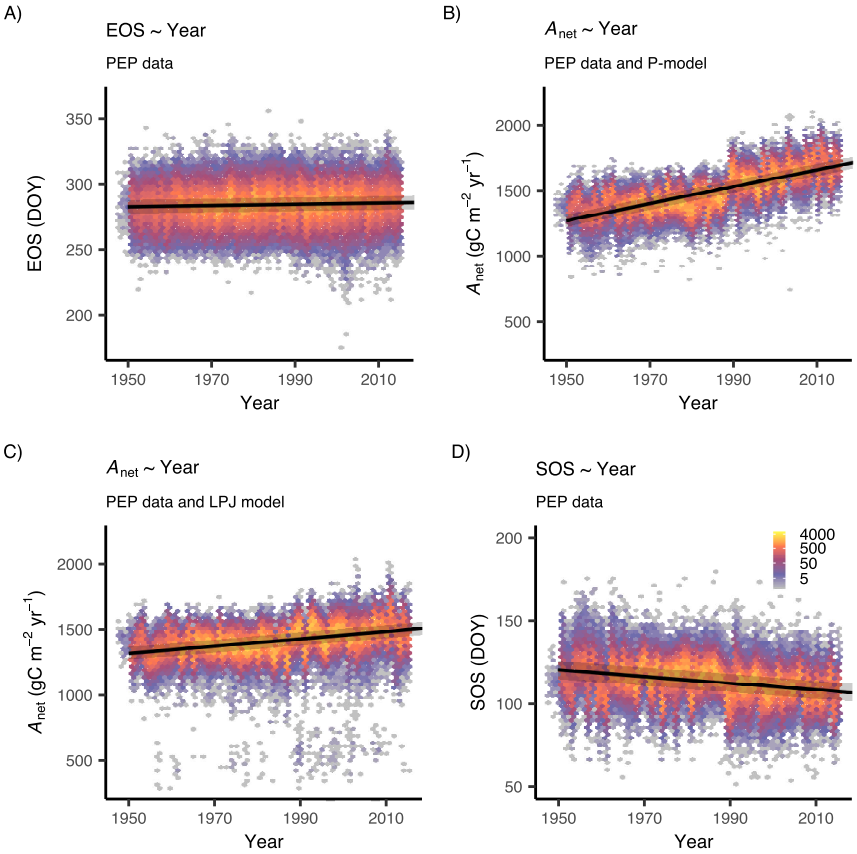

Extended Data Fig. 1 | Temporal trends of CO_2 assimilation and phenological dates from ground observations. (**A**) Trend towards delayed EOS (expressed as day-of-year, DOY), (**B**) increased A_{net} from P-model and (**C**) from LPJ model simulations, and (**D**) advanced SOS (DOY), based on linear mixed-effect models (LMMs) with year as a single fixed effect and site and species as grouping variables of the random intercepts. Black lines represent the expected mean values from LMMs and grey ranges their 95% confidence intervals. Colour hexagonal heatmap represents the observed data adjusted for the effects of the covariates.

https://doi.org/10.1038/s41559-022-01946-1

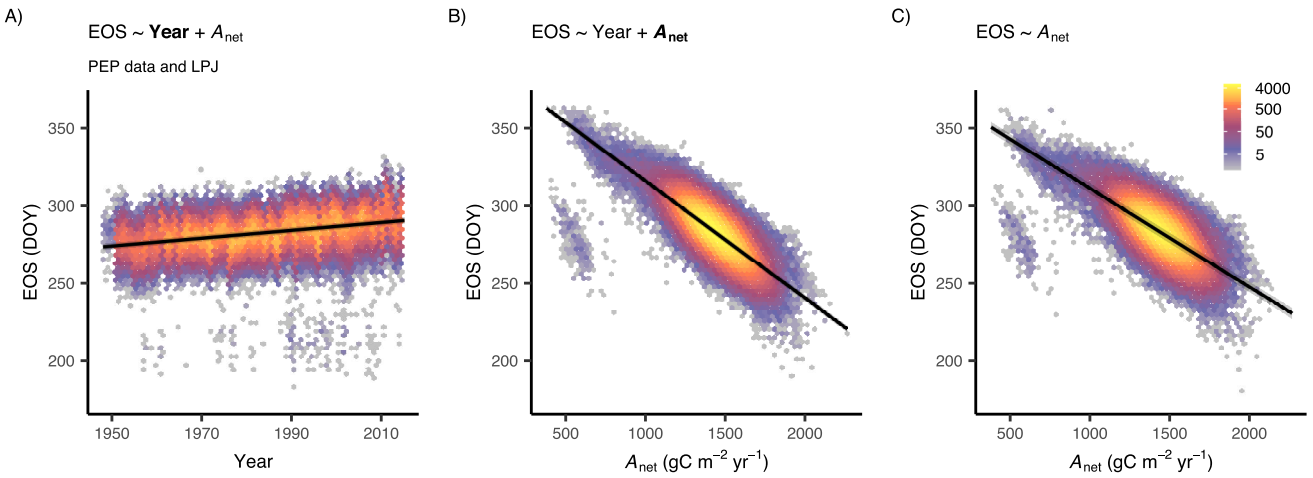

Extended Data Fig. 2 | Relationship of CO_2 assimilation and autumn phenology from ground observations. (**A**, **B**) Partial relationships of a multiple LMM, where EOS is the response variable and (**A**) the long-term trend (year) and (**B**) A_{net} are treated as fixed effects. (**C**) EOS versus A_{net} based on an LMM with A_{net} as a single fixed effect. A_{net} estimates are simulated by the LPJ model. In both bivariate and univariate models, site and species are treated as grouping variables of random intercepts. Black lines represent the expected mean values from LMMs and grey ranges their 95% confidence intervals. Colour hexagonal heatmap represents the observed data adjusted for the effects of the covariates.

https://doi.org/10.1038/s41559-022-01946-1

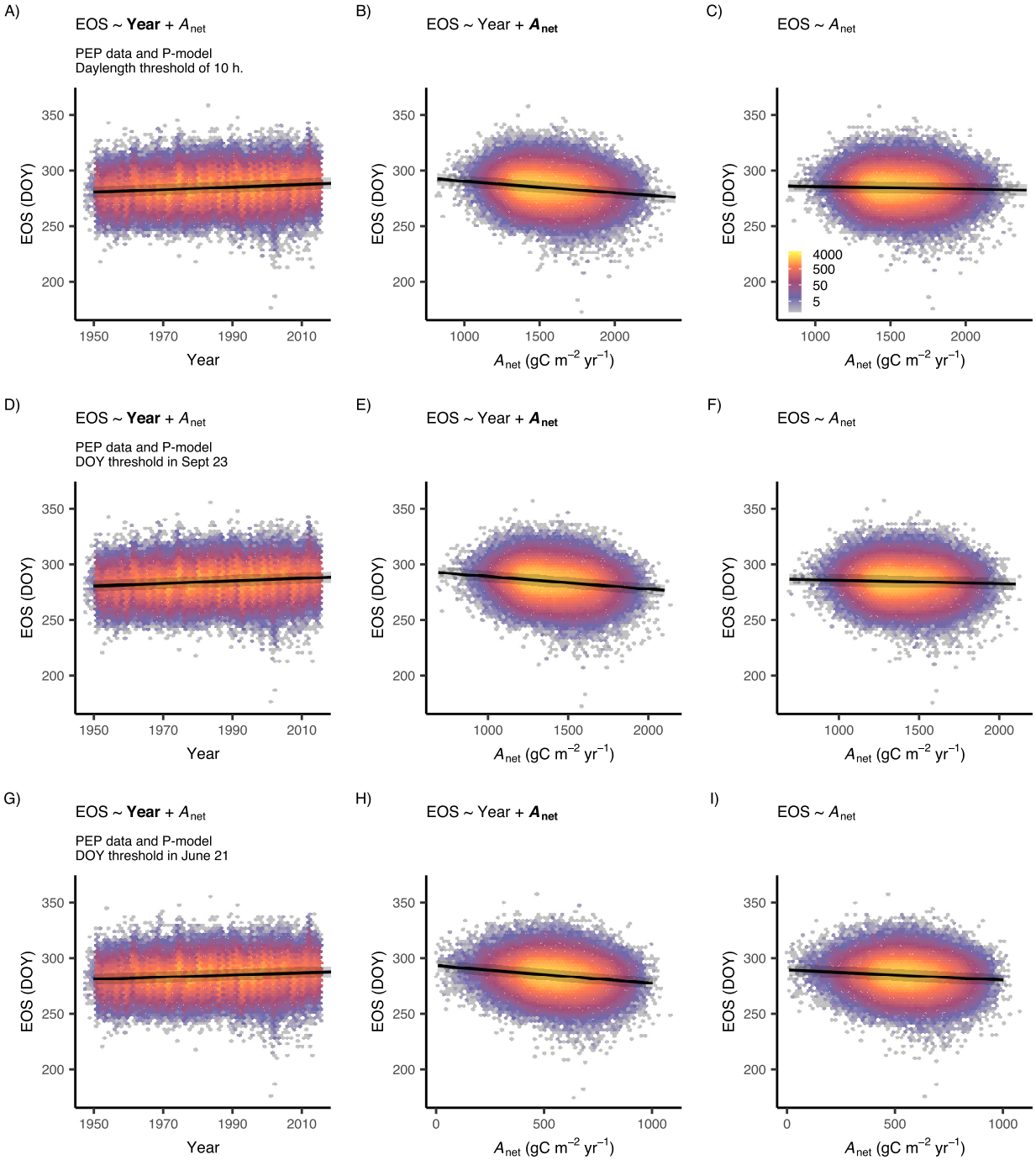

Extended Data Fig. 3 | Sensitivity analysis of the relationship of CO_2 assimilation and autumn phenology from ground observations. Partial relationships of multiple LMMs, where EOS is the response variable and (**A, D, G**) the long-term trend (year) and (**B, E, H**) A_{net} are treated as fixed effects. A_{net} estimates are simulated by the P-model and considering (**B**) a daylength threshold of 10.0 hours, (**E**) a fixed DOY cut-off on the 23rd of September, and (**H**) a fixed DOY cut-off on the 21st of June. (**C, F, I**) EOS versus A_{net} based on an LMM with A_{net} as a single fixed effect. In all bivariate and univariate models, site and species are treated as grouping variables of random intercepts. Black lines represent the expected mean values from LMMs and grey ranges their 95% confidence intervals. Colour hexagonal heatmap represents the observed data adjusted for the effects of the covariates.

https://doi.org/10.1038/s41559-022-01946-1

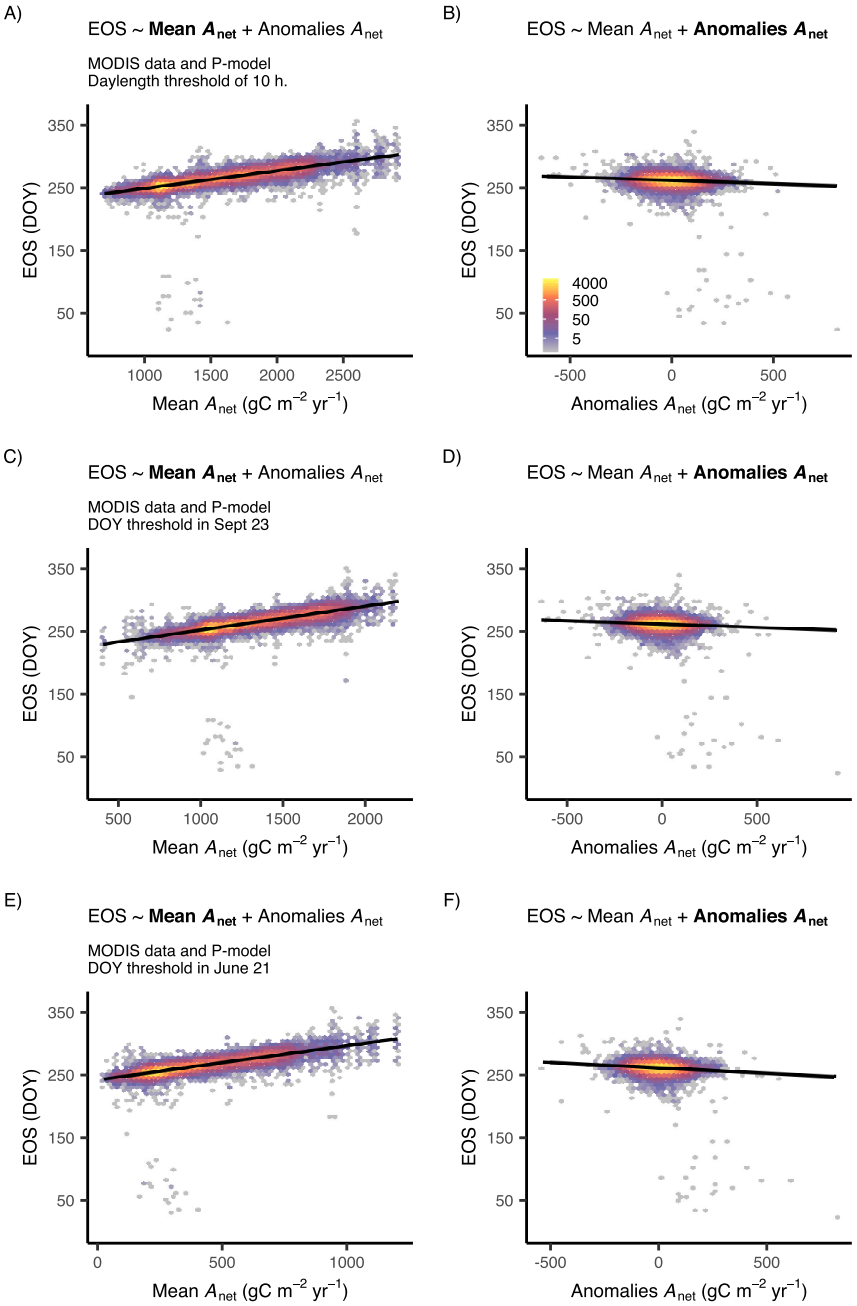

Extended Data Fig. 4 | Sensitivity analysis of the relationship of CO_2 assimilation and autumn phenology from remote-sensing observations. Partial relationships of multiple LMMs, where EOS is the response variable and (**A, C, E**) mean A_{net} and (**B, D, F**) anomalies A_{net} relative to the mean value are treated as fixed effects, while site and year are treated as grouping variables of random intercepts. A_{net} estimates are simulated by the P-model and considering (**A, B,**) a daylength threshold of 10.0 hours, (**C, D**) a fixed DOY cut-off on the 23rd of September, and (**E, F**) a fixed DOY cut-off on the 21st of June. Black lines represent the expected mean values from LMMs and grey ranges their 95% confidence intervals. Colour hexagonal heatmap represents the observed data adjusted for the effects of the covariates.

https://doi.org/10.1038/s41559-022-01946-1

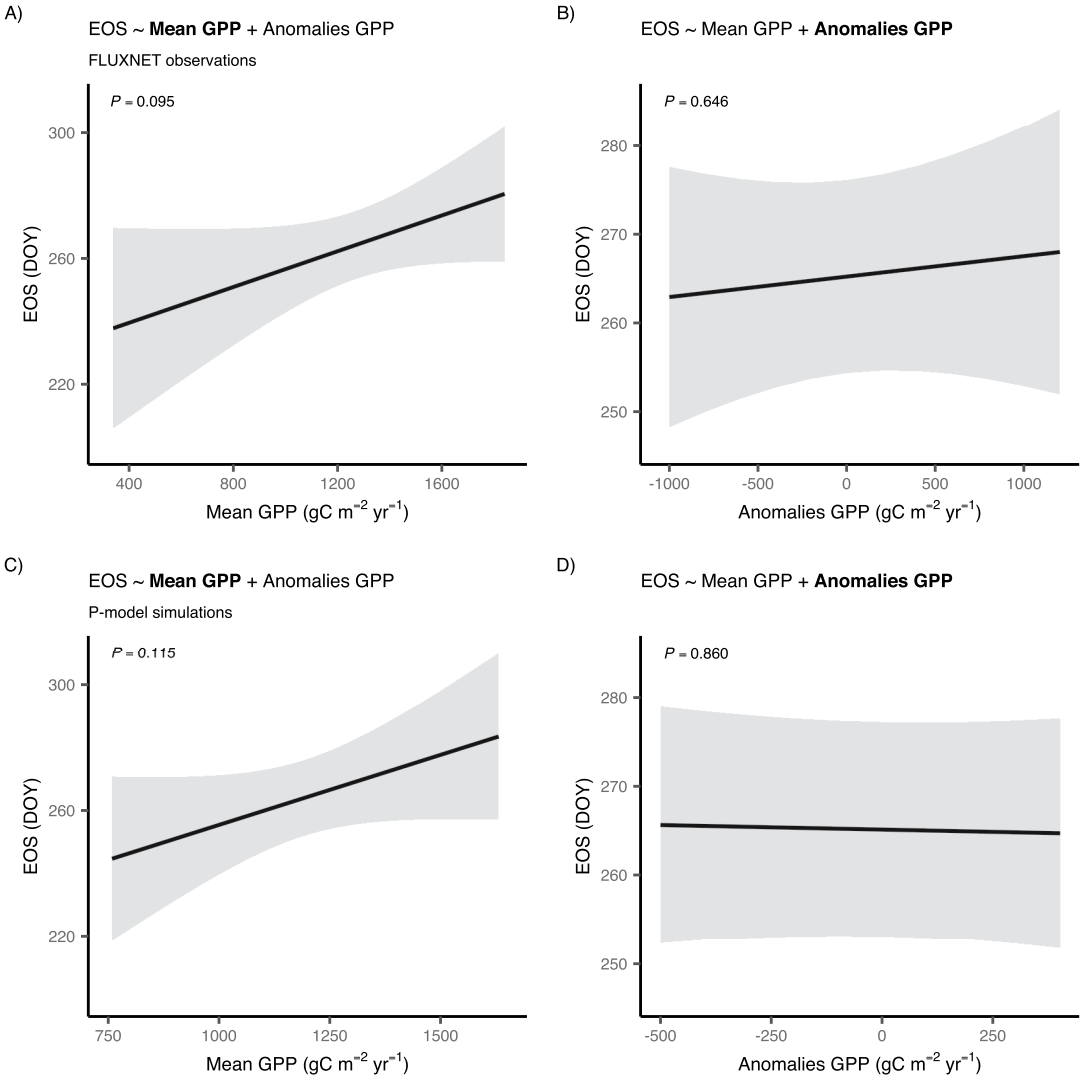

Extended Data Fig. 5 | Comparative relationships of autumn phenology and total gross ecosystem-level CO_2 assimilation from both observations and simulations for the selected FLUXNET sites. Partial relationships of a multiple LMM, with GPP (**A, B**) estimated from FLUXNET 2015 observations or (**C, D**) simulated using the P-model, and where both (**A, C**) mean GPP and (**B, D**) anomalies GPP relative to the mean value are treated as fixed effects, and site and year are treated as grouping variables of random intercepts. Black lines represent the expected mean values from LMMs and grey ranges their 95% confidence intervals.

https://doi.org/10.1038/s41559-022-01946-1

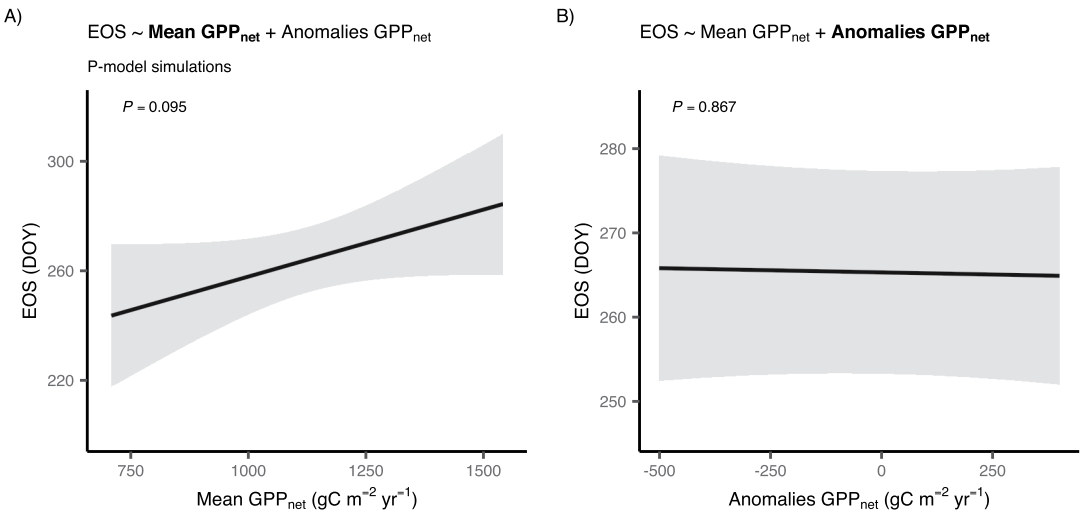

Extended Data Fig. 6 | Relationships of autumn phenology and simulated total net ecosystem-level CO_2 assimilation for the selected FLUXNET sites. Partial relationships of a multiple LMM, with GPP minus ecosystem-level dark respiration (GPP_{net}) simulated using the P-model, and where (**A**) mean GPP_{net} and (**B**) anomalies GPP_{net} relative to the mean value are treated as fixed effects, and site and year are treated as grouping variables of random intercepts. Black lines represent the expected mean values from LMMs and grey ranges their 95% confidence intervals.

https://doi.org/10.1038/s41559-022-01946-1

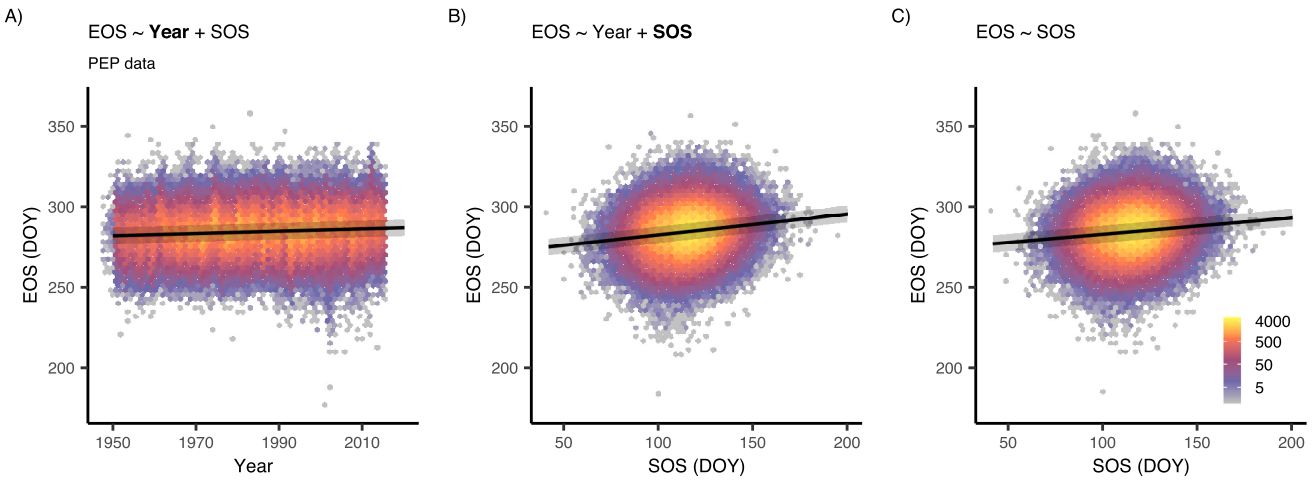

Extended Data Fig. 7 | Relationship of spring and autumn phenological dates from ground observations. (**A, B**) Partial relationships of a multiple LMM, where EOS is the response variable and (**A**) the long-term trend (year) and (**B**) SOS are treated as fixed effects. (**C**) EOS versus SOS based on an LMM with SOS as a single fixed effect. In both bivariate and univariate models, site and species are treated as grouping variables of random intercepts. Black lines represent the expected mean values from LMMs and grey ranges their 95% confidence intervals. Colour hexagonal heatmap represents the observed data adjusted for the effects of the covariates.

https://doi.org/10.1038/s41559-022-01946-1

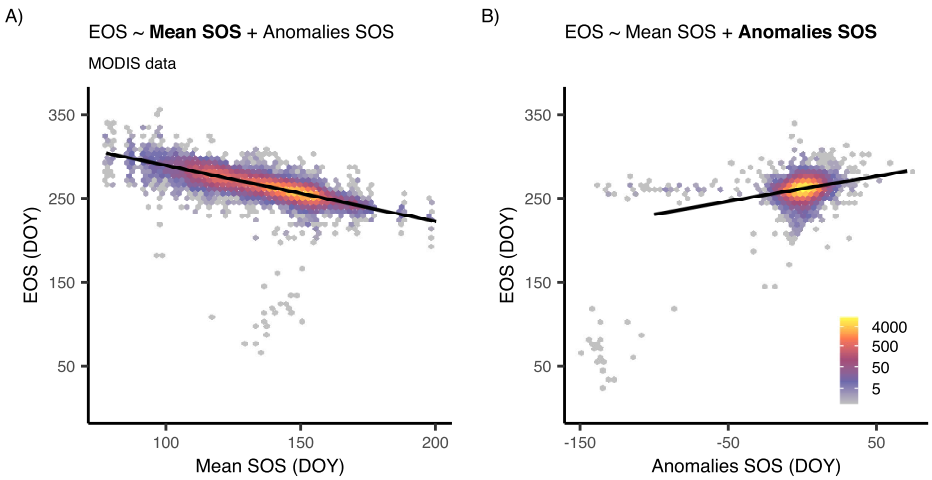

Extended Data Fig. 8 | Relationships of spring and autumn phenological dates from remote-sensing observations. (**A, B**) Partial relationships of a multiple LMM where EOS is the response variable and (**A**) mean SOS and (**B**) anomalies SOS relative to the mean value are treated as fixed effects, and site and year are treated as grouping variables of random intercepts. Black lines represent the expected mean values from LMMs and grey ranges their 95% confidence intervals. Colour hexagonal heatmap represents the observed data adjusted for the effects of the covariates.

https://doi.org/10.1038/s41559-022-01946-1

A)

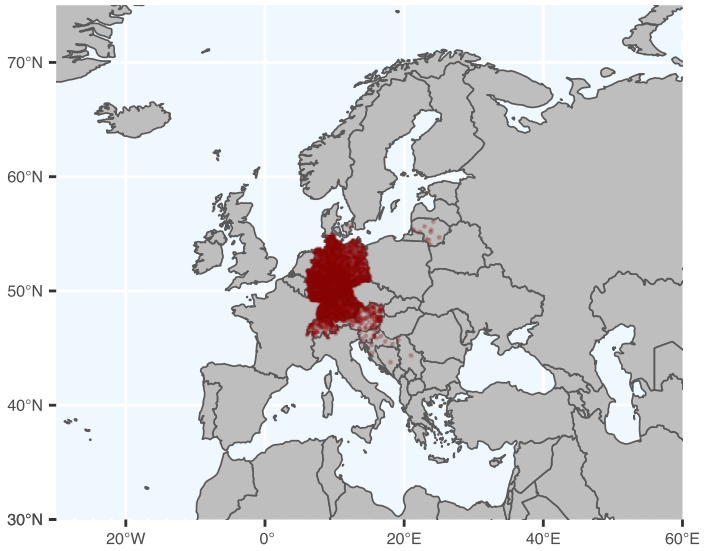

B)

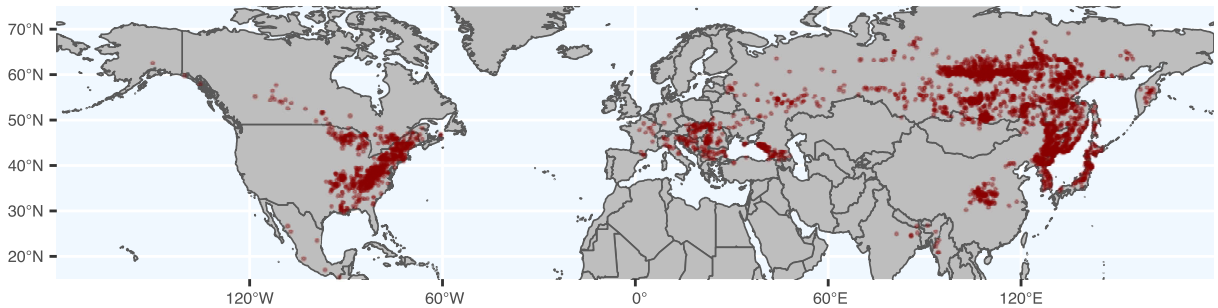

Extended Data Fig. 9 | Site locations of the phenological observations selected from (A) ground and (B) remote-sensing observations. Colour transparency indicates the density of the data points.

nature portfolio

Corresponding author(s): Laura Marques

Last updated by author(s): Oct 24, 2022

Reporting Summary

Nature Portfolio wishes to improve the reproducibility of the work that we publish. This form provides structure for consistency and transparency in reporting. For further information on Nature Portfolio policies, see our Editorial Policies and the Editorial Policy Checklist.

Statistics

For all statistical analyses, confirm that the following items are present in the figure legend, table legend, main text, or Methods section.

n/a	Confirmed	
☐	☒	The exact sample size (*n*) for each experimental group/condition, given as a discrete number and unit of measurement
☐	☒	A statement on whether measurements were taken from distinct samples or whether the same sample was measured repeatedly
☐	☒	The statistical test(s) used AND whether they are one- or two-sided *Only common tests should be described solely by name; describe more complex techniques in the Methods section.*
☐	☒	A description of all covariates tested
☐	☒	A description of any assumptions or corrections, such as tests of normality and adjustment for multiple comparisons
☐	☒	A full description of the statistical parameters including central tendency (e.g. means) or other basic estimates (e.g. regression coefficient) AND variation (e.g. standard deviation) or associated estimates of uncertainty (e.g. confidence intervals)
☐	☒	For null hypothesis testing, the test statistic (e.g. *F*, *t*, *r*) with confidence intervals, effect sizes, degrees of freedom and *P* value noted *Give P values as exact values whenever suitable.*
☒	☐	For Bayesian analysis, information on the choice of priors and Markov chain Monte Carlo settings
☐	☒	For hierarchical and complex designs, identification of the appropriate level for tests and full reporting of outcomes
☒	☐	Estimates of effect sizes (e.g. Cohen's *d*, Pearson's *r*), indicating how they were calculated

Our web collection on statistics for biologists contains articles on many of the points above.

Software and code

Policy information about availability of computer code

Data collection	Code for the data analysis of this study is available at the Github repository DOI:10.5281/zenodo.5799642
Data analysis	The analyses were performed using the R statistical software version 4.0.5.

For manuscripts utilizing custom algorithms or software that are central to the research but not yet described in published literature, software must be made available to editors and reviewers. We strongly encourage code deposition in a community repository (e.g. GitHub). See the Nature Portfolio guidelines for submitting code & software for further information.

Data

Policy information about availability of data

All manuscripts must include a data availability statement. This statement should provide the following information, where applicable:

- Accession codes, unique identifiers, or web links for publicly available datasets
- A description of any restrictions on data availability
- For clinical datasets or third party data, please ensure that the statement adheres to our policy

Ground phenology data provided by the members of the Pan European Phenology Project (PEP725) is freely available at http://www.pep725.eu. Remote-sensing phenology data from the MODIS C6 MCD12Q2 Land Surface Dynamics Product is freely accessible at https://lpdaac.usgs.gov/products/mcd12q2v006/. Eddy covariance data are freely available by the FLUXNET community at https://fluxnet.org.

Field-specific reporting

Please select the one below that is the best fit for your research. If you are not sure, read the appropriate sections before making your selection.

☐ Life sciences ☐ Behavioural & social sciences ☒ Ecological, evolutionary & environmental sciences

For a reference copy of the document with all sections, see nature.com/documents/nr-reporting-summary-flat.pdf

Ecological, evolutionary & environmental sciences study design

All studies must disclose on these points even when the disclosure is negative.

Study description	Our study focuses on understanding the relationships between autumn phenology, net photosynthesis and spring leaf-out across different spatio-temporal scales. We use multi-decadal ground and remote-sensing observations to investigate these relationships at the interannual, long-term, and spatial scales.
Research sample	Deciduous tree species in temperate and boreal forests.
Sampling strategy	The PEP725 dataset resulted in 3,855 sites across Central Europe with 14,626 individual time series and 434,226 phenological observations. The MODIS C6 MCD12Q2 dataset provided 4,879 randomly sampled points of deciduous tree species in temperate and boreal forests.
Data collection	We used ground observations of spring and autumn phenology dates from the PEP725, and remote-sensing data from the MODIS C6 MCD12Q2 Land Surface Dynamics Product. Gross primary production (GPP) data was collected from the FLUXNET 2015 Tier 1 dataset.
Timing and spatial scale	The PEP725 dataset provided multi-year ground observations for Europe from the period 1948-2015. Remotely sensed estimates from MODIS C6 MCD12Q2 included randomly sampled points of deciduous tree species during the period 2001-2018. Observational data from the FLUXNET 2015 was provided from 2000 to 2014.
Data exclusions	From the PEP725 dataset, we selected deciduous forests and time series with more than 15 years of observations. From the MODIS dataset, we selected the pixels corresponding to the Northern Hemisphere. From the FLUXNET 2015 we selected sites categorized as as broadleaf deciduous (DBF), needleleaf deciduous (DNF) and mixed forests (MF) based on the International Geosphere–Biosphere Programme (IGBP) definition.
Reproducibility	Code to reproduce the results of this study is available at the Github repository DOI:10.5281/zenodo.5799642. No experiments were conducted.
Randomization	For the PEP725 and FLUXNET 2015 observations, site-given data was considered. For the MODIS dataset, we randomly sampled 5,000 pixels spread evenly between temperate deciduous needle and broadleaf IGBP classes and selected the points corresponding to the Northern Hemisphere.
Blinding	Blinding was not relevant for our study since we used phenological observations.

Did the study involve field work? ☐ Yes ☒ No

Reporting for specific materials, systems and methods

We require information from authors about some types of materials, experimental systems and methods used in many studies. Here, indicate whether each material, system or method listed is relevant to your study. If you are not sure if a list item applies to your research, read the appropriate section before selecting a response.

Materials & experimental systems

n/a	Involved in the study
☒	☐ Antibodies
☒	☐ Eukaryotic cell lines
☒	☐ Palaeontology and archaeology
☒	☐ Animals and other organisms
☒	☐ Human research participants
☒	☐ Clinical data
☒	☐ Dual use research of concern

Methods

n/a	Involved in the study
☒	☐ ChIP-seq
☒	☐ Flow cytometry
☒	☐ MRI-based neuroimaging